MARTIAN POLAR CLOUDS.

P. G. Ford and G. H. Pettengill[1],
[1]Center for Space Research, MIT 37–571, 77 Massachusetts Avenue, Cambridge, MA 02139-4307, USA
<pgf@space.mit.edu>

Introduction: The Mars Orbiting Laser Altimeter (MOLA) instrument [1,2] carried aboard the Mars Global Surveyor (MGS) spacecraft, has observed echoes from cloud tops at 1.064μm on 61% of its orbital passes over the winter north pole ($235° < L_s < 315°$) and on 58% of the passes over the winter south pole ($45° < L_s < 135°$). The clouds are unlikely to be composed of water ice since the vapor pressure of H_2O is very low at the Martian nighttime polar temperatures measured by TES, the Thermal Emission Spectrometer [3], and by an analysis of MGS radio occultations [4]. Dust clouds can also be ruled out since no correlation is seen between clouds and global dust storms. The most likely candidate is CO_2 ice.

We have constructed a database of MOLA clouds, identified by clusters of closely grouped echoes. Each set of cloud echoes was plotted by altitude and along-track distance (see Figs. 3–5), inspected visually, and assigned to a category by its morphology and relation to surface features. The location of clouds by latitude, sub-solar longitude (L_s), and solar incidence angle are shown in Figs. 1 and 2.

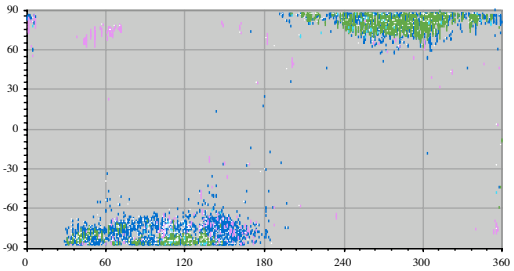

Fig. 1: Location of MOLA clouds by latitude and sub-solar longitude (L_S).

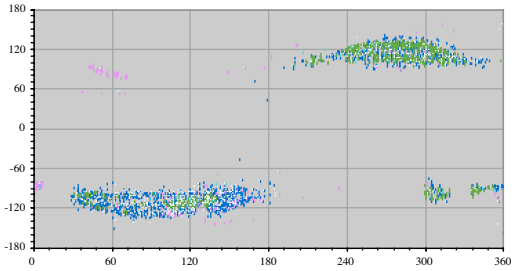

Fig. 2: Location of MOLA clouds by solar incidence angle and sub-solar longitude (L_S).

The colors used to denote the cloud locations in Figs. 1 and 2 indicate the categories that we have assigned to them, as exemplified Figs. 3–5 which show the altitude (km) and distance-along-track (km) of individual lidar echoes for the three most common categories.

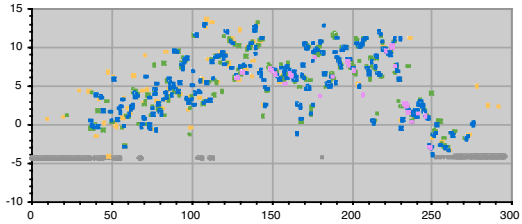

Fig. 3: Echoes from a typical cloud formation that is adjudged to contain *propagating* waves—green in Figs. 1 and 2—which are more common in north than in south polar regions.

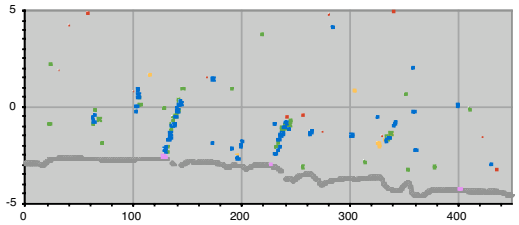

Fig. 4: Example of clouds associated with *topographic* features—colored blue in Figs. 1 and 2—with the appearance of mountain waves or perhaps snow tails.

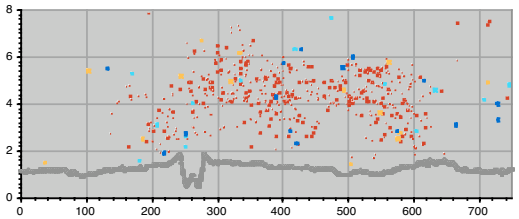

Fig. 5: Example of *diffuse* clouds—colored red in Figs. 1 and 2—whose lidar echoes show very little time dispersion. They are seen only in southern polar latitudes.

The less common categories are *dome-shaped* (colored light blue in Figs. 1 and 2), dense isolated formations not apparently associated with surface features, *ground-hugging* clouds (magenta), flat clouds that form at altitudes of less than 1 km in the spring and autumn dawn, and *crater clouds* (brown), which form within large impact craters.

The data points in Figs. 3–5 have been color coded according to the time dispersion of the lidar echoes: red indicates reflection from a cloud top whose density

varies strongly over no more than 3m of range; green and yellow denote intermediate thicknesses, while the blue echoes are the most dispersed in range—from clouds whose density changes over 90m or more. Cloud echoes that saturated the MOLA receiver are colored magenta, and surface echoes are colored grey.

Under conditions of Mie scattering and assuming unit geometric albedo, the density of CO_2 ice particles required to produce the observed echo strengths is about $2\times10^{8}\ r^{-2}\ m^{-3}$, where r is the particle radius in μm, which we infer to lie between 0.1μm and 50 μm. If $r < 0.1$μm, Rayleigh scattering will predominate, the cross-section will vary as r^{-4}, and no lidar echo would be detectable. If $r > 50$μm, the particles would fall too fast to sustain the observed wave patterns.

In addition to these reflective clouds, MOLA often receives no echo from either cloud or surface. These *non-reflective* clouds form a distinct category. Since they are not exclusive to the polar night, and are more common during hemispheric dust storms, they may be composed largely of dust rather than CO_2 or H_2O.

Buoyancy Waves. We have identified and measured all lineaments within the cloud-top echoes, such as those visible in Figs. 3 and 4. We assume that the multiple wave fronts of the *propagating* class (Fig. 3) are buoyancy waves moving through a CO_2 atmosphere [5]. Particles of dry ice are alternately condensed and evaporated as the ambient temperature is modulated above and below the local freezing point by the passing wave. This implies that the atmosphere is close to its "wet,, CO_2 adiabat at ~148K, at which point the buoyancy frequency is estimated to be $\sim9.31\times10^{-3}$ rad s^{-1}.

Spatial-Temporal Correlation. The combination of the MGS sun-synchronous orbit period, ~7060.72 s and the length of the Martian day, ~88774.9 s, results in near overlap of tracks at 7-day (22 orbit) intervals. However, since the tracks converge at ±86° latitude, more frequent overlaps will occur in polar latitudes. We therefore correlated the locations of all clouds of a given category with each other, assuming that they rotate in common around their pole with a mean zonal flow. Fig. 6 shows the result of these correlations around the south pole, for a range of zonal rotation rates.

Note the strong correlation at non-zero rotation rate for the class of *propagating* clouds (*e.g.*, Fig. 3) and the relatively weak correlation between clouds related to *topographic* features (e.g., Fig. 4), suggesting that the former are moving in a polar vortex—*ca*. 5 m s^{-1} at 75°S latitude—while the latter are not. The tracks of some correlated propagating clouds are shown in Fig. 7.

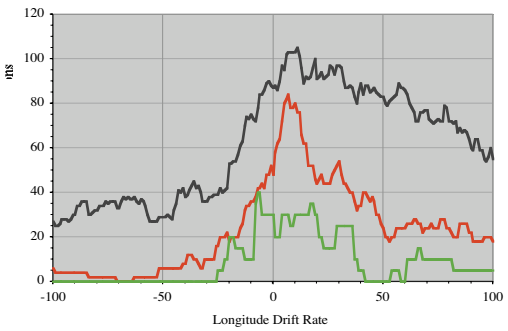

Fig. 6: correlation between pairs of clouds detected within 48 hours of each other and separated by < 1° of arc measured from the center of body, after a constant zonal wind (degrees of longitude per day) has been removed. Red: correlation of propagating clouds; green: of topographic clouds; black: of all cloud categories.

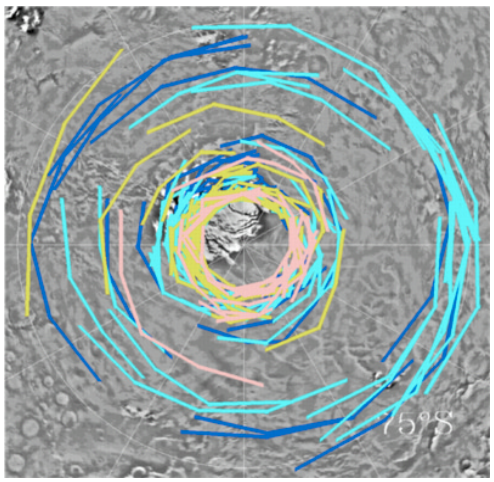

Fig. 7: Correlated clouds over the south pole. Color denotes the correlation interval, pink: 1 day; green: 2 days; blue: 3 days; cyan: 4 days.

Infrared Emission. Simultaneous observations were made by MOLA and by the MGS Thermal Emission Spectrometer (TES) [6]. At the low temperatures of the polar night, the emission spectrum E(λ) between 15μm and 25μm is most useful. With minimal contribution from H_2O and dust, the emission is dominated by the CO_2 rotation band at 15μm and by the thermal (Planck) spectrum from the surface and atmosphere at their respective temperatures. Although the fundamental spatial resolution of each of the 6 TES detectors is ~3×3 km, the six are usually summed together for polar nighttime observations in order to achieve adequate SNR. Each footprint is therefore ~6×9 km and encloses the ~200 m diameter MOLA footprint. The surface emissivity is typically ~0.95 at these wavelengths, so typical TES observations in the polar

night (see Fig. 8) show an atmosphere and surface at ~148K.

Anomalous "cold spots,, have been observed in the polar night, both by TES and by the IRIS instrument on Mariner 9 [7]. Fig. 8 shows TES spectra at three latitudes. On the left, at 60°S, the warm sunlit atmosphere emits strongly at 15µm, but it is almost transparent at other wavelengths, which are dominated by surface emission. At 85.5°S, the atmosphere is colder than the surface and absorbs at 15 µm, while the radiometric temperature drops at $\lambda > 20\mu m$, indicating a "cold spot,,. At 79.5°S, the long-wavelength anomaly disappears and only the 15µm absorption feature remains.

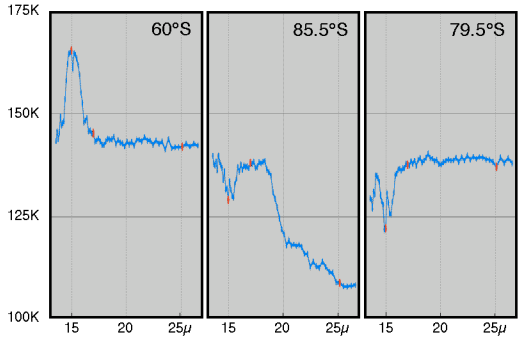

Fig. 8: Infrared TES emission spectra at three latitudes in the same pass (orbit 18799, $L_s = 122°$).

Three models have been put forward to explain the cold spots. They could result from CO_2 ice clouds [8], from a deep layer of CO_2 frost [8,9], or from surface layers of CO_2 slab ice [10]. In each case, the emissivity is lowered by volume scattering, but in very different conditions. To choose between these models, we have made maps of the spectral slope, $\partial E/\partial\lambda$, for $20\mu m < \lambda < 25\mu m$ at intervals of 5° in L_s. The cold spots show up clearly as isolated minima, as in Fig. 9.

Having identified a particular cold spot, we have noted the first time at which TES detected it and the last time, if any, at which TES observed that region without detecting any anomaly. From this, an estimate of the average lifetime of a cold spot can be determined. We go on to correlate MOLA clouds with TES cold spots to see whether the two are related, and whether particular types of cloud are responsible.

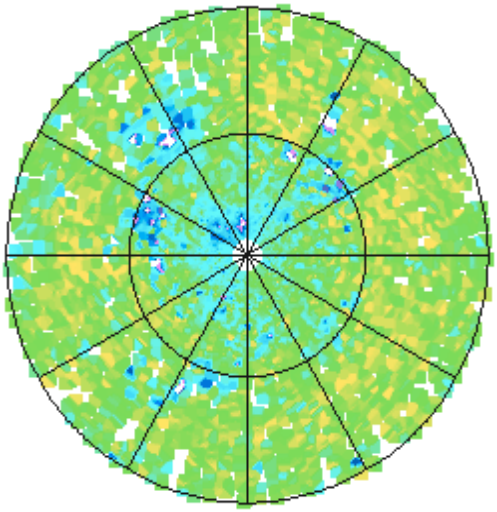

Fig. 9: Map of the TES spectral slope, $\partial E/\partial\lambda$, for $20\mu m < \lambda < 25\mu m$, $70° < L_S < 80°$ in the southern winter. Cold spots (blue, magenta) are clearly visible with negative spectral slopes.

This work, funded under NASA grant NAG5-4434, is still in progress. A copy of the material to be presented at the workshop will be made available for download from ftp://voir.mit.edu/granada2003.

[1] Zuber *et al.,* J. Geophys. Res., 97, 7781 (1992)
[2] Zuber *et al.,* Science, 282, 2053 (1998)
[3] Christensen *et al.,* J. Geophys. Res., 106, 23823 (2001)
[4] Hinson *et al.,* J. Geophys. Res., 106, 1463 (2001)
[5] Pettengill and Ford, Geophys. Res. Lett., 27, 609 (2000)
[6] Pearl *et al.,* J. Geophys. Res., 106, 12325 (2001)
[7] Hanel *et al.,* Icarus, 17, 423 (1972)
[8] Forget *et al.,* J. Geophys. Res., 100, 21219, (1995)
[9] Ditteon and Kieffer, J. Geophys. Res., 84, 8294 (1979)
[10] Titus et al., EOS Trans., 80, 611 (1999)